Matthias Roth, Jörg Heber, Klaus Janschek

System design of programmable 4f phase modulation techniques for rapid intensity shaping: a conceptual comparison

Erstveröffentlichung in / First published in:

SPIE LASE. San Francisco, 2016. Bellingham: SPIE, Vol. 9736 *[Zugriff am: 02.05.2019].*

DOI: https://doi.org/10.1117/12.2210917

System design of programmable 4f phase modulation techniques for rapid intensity shaping: a conceptual comparison

Matthias Roth, Jörg Heber, Klaus Janschek

Matthias Roth, Jörg Heber, Klaus Janschek, "System design of programmable 4f phase modulation techniques for rapid intensity shaping: a conceptual comparison," Proc. SPIE 9736, Laser-based Micro- and Nanoprocessing X, 97361G (4 March 2016); doi: 10.1117/12.2210917

SPIE.

Event: SPIE LASE, 2016, San Francisco, California, United States

System design of programmable 4f phase modulation techniques for rapid intensity shaping - a conceptual comparison

Matthias Roth[a], Jörg Heber[b], and Klaus Janschek[a]

[a]Technische Universität Dresden, Institute of Automation, 01062 Dresden, Germany
[b]Fraunhofer Institute for Photonic Microsystems, Maria-Reiche-Str. 2, 01109 Dresden, Germany

ABSTRACT

The present study analyses three beam shaping approaches with respect to a light-efficient generation of i) patterns and ii) multiple spots by means of a generic optical 4f-setup. 4f approaches share the property that due to the one-to-one relationship between output intensity and input phase, the need for time-consuming, iterative calculation can be avoided. The resulting low computational complexity offers a particular advantage compared to the widely used holographic principles and makes them potential candidates for real-time applications. The increasing availability of high-speed phase modulators, e.g. on the basis of MEMS, calls for an evaluation of the performances of these concepts.
Our second interest is the applicability of 4f methods to high-power applications. We discuss the variants of 4f intensity shaping by phase modulation from a system-level point of view which requires the consideration of application relevant boundary conditions. The discussion includes i) the micro mirror based phase manipulation combined with amplitude masking in the Fourier plane, ii) the Generalized Phase Contrast, and iii) matched phase-only correlation filtering combined with GPC. The conceptual comparison relies on comparative figures of merit for energy efficiency, pattern homogeneity, pattern image quality, maximum output intensity and flexibility with respect to the displayable pattern. Numerical simulations illustrate our findings.

Keywords: spatial light modulator, Fourier optics, generalized phase contrast

1. INTRODUCTION

Spatial beam shaping plays an important role in a variety of applications - from optical micromanipulation or structured lighting in microscopy to direct laser writing and additive techniques in production. Spatial light modulators (SLMs) are modern optical elements that enable the programmable modulation of light in space, which generates flexibility and throughput compared to single spot scanning solutions. SLM techniques can be used for direct laser writing of patterns or the creation of multiple foci, without the need for serial mechanical scanning. In this work we consider SLM shaping methods because of their high speed and light efficiency capabilities. We limit our discussion to phase-only light modulators, based on the efficiency boundary. For a discussion of amplitude modulation techniques, for example Digital Micromirror Device (DMD) based setups for direct laser transfer,[1] we direct the reader to comprehensive reviews in this field.[2]

Phase-only SLMs can be used for pattern shaping in the so-called 2f configuration, by placing the SLM and the target in consecutive focal planes of a single lens. To determine the phase function for a desired intensity pattern, numerous works use an iterative approach (Iterative Fourier Transform Algorithm, IFTA)[3] to construct a phase input for a desired intensity modulation. Iterative optimization leads to a multitude of free design parameters and results in significant computational loads. Several works address this problem by using specialized hardware (find references in Ref. 4) and software methods.[5] Optimized light efficiency requires the usage of high spatial frequencies and therefore spatially fast varying output patterns commonly termed as speckle.[4] Adaptations to IFTA address this issue.[6]

Further author information: (Send correspondence to M.R.)
E-mail: matthias.roth@tu-dresden.de, Telephone: +49 351 46332243

Laser-based Micro- and Nanoprocessing X, edited by Udo Klotzbach, Kunihiko Washio, Craig B. Arnold,
Proc. of SPIE Vol. 9736, 97361G · © 2016 SPIE · CCC code: 0277-786X/16/$18 · doi: 10.1117/12.2210917

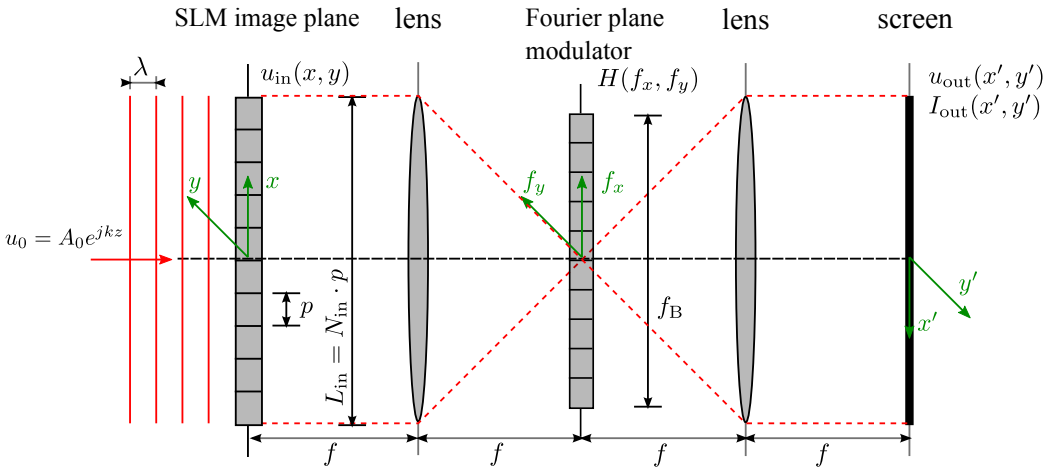

Figure 1: Generic optical 4f setup with transmission filters. The input modulator has a side length L_{in} consisting of N_{in} pixels of pitch p. The Fourier plane bandwidth is f_{B}. Light fields are denoted by u_{in} at the input, H for the Fourier plane modulation and the output field u_{out}. The optical propagation through two consecutive lenses leads to an inversion of the coordinates between input and output.

In this paper our interest concentrates on a so-called optical 4f-configuration. It consists of two lenses and two modulators placed in consecutive focal planes (see fig.1). The input-output relationship of this setup is analytic and therefore no online calculation is needed. A prominent, industrial grade method for intensity modulation using a 4f-setup is the SLM imaging for maskless lithography. This technique relies on a 4f-setup with a static amplitude filter in the Fourier plane and features high update rates due to its low computational complexity (see sec.3.1). System design aspects have been investigated in previous works.[7,8]

The Generalized Phase Contrast method (GPC, sec.3.2)[9] uses a static phase filter in the 4f Fourier plane. Due to its restriction to phase-only-modulation in both image and Fourier plane it enables high energy efficiencies[10] and thereby promises enhanced optical performance.[11] In this paper we consider the system level requirements for the construction of a versatile pattern imaging setup on the basis of GPC. We assume that the desired pattern may cover a variable modulation area. This aspect is reflected by the so-called pattern fill factor. Furthermore, we emphasize that for an universal imaging setup the relevant target pattern may possess an arbitrary symmetry or asymmetry. Therefore, we go beyond studies that considered system aspects of symmetric patterns only.[12] Simulations quantify the influence of the variable pattern fill factor and the optical alignment on the GPC system design.

After examining the generation of continuous patterns in section 3, we discuss the creation of multiple light spots in section 4. It makes use of the so-called matched phase filtering,[13] a technique originating from signal processing. It has already been combined with GPC[14] to create high intensity spots at high modulation speed and light efficiency. We consider its system level requirements and demonstrate the feasibility of a fast modulator technology in the input plane.

2. SIMULATION CONCEPT

Today, various types of phase modulators are used for intensity shaping. Our main interest lies in the modulation speed, therefore we consider pixelated MEMS of two types that may support kilohertz framerates. Piston type reflective SLMs[15] (fig. 2a) introduce a phase shift by changing the optical path length with respect to neighboring pixels. Tilt micro mirror arrays (MMAs) (fig. 2b) exhibit one rotational degree of freedom per pixel with an analog tilt angle θ.[16] Both geometries can be driven by different actuator types. Independent of the pixel geometry, the constructed phase Φ is given by the optical path difference and the wave number $k = \frac{2\pi}{\lambda}$

$$\Phi(x) = -2kh(x) \ . \tag{1}$$

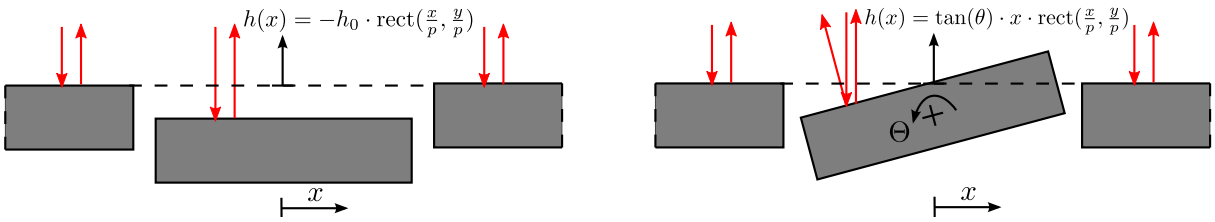

(a) Piston mirror (b) Tilt mirror

Figure 2: Reflective phase SLM types, with respective height profiles $h(x, y)$ for a single pixel of size $p \cdot p$

As discussed above we restrict ourselves to phase-only modulation of the input field u_{in}. In the most general case the Fourier plane filter H can be a complex filter. The setups we consider differ in their Fourier plane Filter $H(f_x, f_y)$, which may be a phase or amplitude filter. Without loss of generality the modulation area is assumed to be quadratic.

The effective resolution of a 4f setup will depend on the optical apertures. Therefore, as typical design parameter we consider the spatial bandwidth in the Fourier plane f_{B} (see fig. 1). It places a limit to the effective resolution, because spatial frequency portions larger than $0.5\, f_{\mathrm{B}}$ do not propagate from the input to the output plane.

Within the following simulations, the complex fields in the focal planes of the two consecutive lenses will be our primary interest. The input-output-relationship comprises two consecutive Fourier transforms (Fraunhofer diffraction):[17]

$$u_{\mathrm{out}}(x', y') = \mathfrak{F}\{H(f_x, f_y) \cdot \mathfrak{F}\{u_{\mathrm{in}}(x, y)\}\} \ . \tag{2}$$

We denote the Fourier plane coordinates in spatial frequency coordinates (f_x, f_y) - physical dimensions in the Fourier plane $(x_{\mathrm{F}}, y_{\mathrm{F}})$ correspond to $(x_{\mathrm{F}}, y_{\mathrm{F}}) = \lambda f \cdot (f_x, f_y)$.[17]

The parameterization of our simulation examples is governed by three numerical constraints. Since we investigate the image quality of modulation methods in the spatial domain we choose our sampling resolution in the spatial domain 10 times smaller than the modulator pixel pitch p. In addition, we require a precise sampling interval in the frequency domain in order to investigate the GPC Fourier filter properties. Since the GPC filter is applied to zero order diffraction we sample this diffraction order of our rectangular aperture with 20*20 samples. We achieve this fine sampling in the frequency domain by means of zero-padding of the complex fields.[18] In our simulations, zero-padding is used to a higher degree than necessary for most optical propagation computations.[19] In our calculation array for the input field u_{in} zero-padding takes up 99.76 % of the calculation area to achieve the desired spatial frequency resolution. Our pattern examples consist of 40*40 modulator pixels. This is the largest input size for which both sampling constraints are satisfied and for which a standard PC with 16 GByte RAM can compute the corresponding complex Fourier transforms using Matlab$^{\mathrm{TM}}$

$$\text{pixel pitch} : p = 20\,\mu\mathrm{m},\ \text{spatial sampling} : \Delta x = 2\,\mu\mathrm{m},\ N_{\mathrm{in}} = 40\ ,\ L_{\mathrm{in}} = N_{\mathrm{in}} \cdot p = 800\,\mu\mathrm{m},\ \lambda = 500\,\mathrm{nm}$$

$$\text{Fourier plane sampling} : \Delta f_{\mathrm{simulation}} = \frac{1}{N_{\mathrm{simulation}} \cdot \Delta x} \overset{!}{<} \frac{1}{20}\frac{1}{L_{\mathrm{in}}}$$

$$\text{Fourier Transform array size in simulation } N^2_{\mathrm{simulation}} = 8192 \cdot 8192\ .$$

3. PATTERN GENERATION

This section deals with 4f-methods designed to project arbitrary, continuous image patterns. At first, we discuss a classical tilt micro mirror technique with amplitude filtering in sec. 3.1 and consider the Generalized Phase Contrast in section 3.2, which promises higher light efficiency.

Figures of merit in our discussion evaluate the intensity in the output plane I_{out} in eqs.(3,4,5). The output pattern quality can be characterized by the mean intensity $\overline{I}_{\text{pattern}}$ and the standard deviation σ_{pattern} within the pattern area. It is typically desired to also evaluate the light modulation in areas outside the main target pattern, here illustrated by its mean $\overline{I}_{\text{dark}}$. Both techniques we analyze offer grayscale capability, but for the ease of analysis we demonstrate only patterns with a uniform desired amplitude in this paper.

In order to assess the energy efficiency of 4f systems we determine the efficiency coefficient ϵ, calculated from the total light directed to the image pattern and the total intensity at the input modulator in eq.(6)

$$\overline{I}_{\text{pattern}} = \text{mean}\left(I_{\text{out}}(x',y')|_{(x',y')\in \text{ pattern}} \right) \tag{3}$$

$$\overline{I}_{\text{dark}} = \text{mean}\left(I_{\text{out}}(x',y')|_{(x',y')\notin \text{ pattern}} \right) \tag{4}$$

$$\sigma_{\text{pattern}} = \text{std}\left(I_{\text{out}}(x',y')|_{(x',y')\in \text{ pattern}} \right) \tag{5}$$

$$\epsilon = \frac{\iint I_{\text{out}}(x',y')|_{(x',y')\in \text{ pattern}}\, \mathrm{d}x'\mathrm{d}y'}{\iint I_{\text{in}}(x,y)\, \mathrm{d}x\mathrm{d}y} \ . \tag{6}$$

3.1 Tilt Micro Mirror Array (MMA) for image generation

Micromirror arrays may form a programmable grayscale mask[7,16] with a static amplitude filter in the Fourier plane. The input phase of the tilt mirror array is a saw-tooth phase grating, where the angle of each pixel Θ_i at position $(x_{\text{p},i}, y_{\text{p},i})$ can be individually controlled (eq.(7)). The grayscale output intensity is determined as a direct function of the tilt angle (eq.(8)). If the mirror edge deflection reaches a quarter of the wavelength (the blaze condition), virtually all light modulated by this pixel will be diffracted to the first diffraction order of the programmable grating, located at the spatial frequency $\pm 1/p$.[16] A spatial amplitude filter in the Fourier plane excludes the first and higher diffraction orders from the imaging path. We describe the aperture of the amplitude filter with the normalized, dimensionless factor ζ (see eq.(9)). Partial coherent imaging conditions usually lead to filter sizes in the order of $\zeta \approx 0.5$ or smaller

$$\Phi_{\text{in}}(x,y) = (-2k)\cdot \sum_{i=1}^{N_{\text{in}}^2} \tan(\Theta_i)\cdot x \cdot \text{rect}\left(\frac{x-x_{\text{p},i}}{p}, \frac{y-y_{\text{p},i}}{p} \right) \tag{7}$$

$$I_{\text{out}}(x'=x_{\text{p},i}, y'=y_{\text{p},i}) \propto \text{sinc}^2\left(\frac{2\pi\cdot p\cdot \tan(\Theta_i)}{\lambda} \right) \cdot I_{\text{in}}(x=x_{\text{p},i}, y=y_{\text{p},i}) \tag{8}$$

$$H_{\text{MMA}}(f_x,f_y) = \text{rect}\left(\frac{f_x}{2\zeta p^{-1}}, \frac{f_y}{2\zeta p^{-1}} \right) \ \text{ with } \zeta \in \ [0,1] \ . \tag{9}$$

Figure 3 shows the typical numerical result of a MMA pattern simulation. A clear distinction of the pattern from the surrounding area and a nearly uniform spatial intensity distribution of the output pattern can be seen. Deviations from the desired pattern originate from the low pass filtering. For a discussion of the possible contrast metrics under practical conditions we direct the reader to experimental studies elsewhere.[8]

Since this technique uses an amplitude filter, the output intensity never will surpass the source intensity. The energy efficiency is limited by the pattern fill factor. The effective image resolution is determinded by the filter size ζ (low-pass filter).

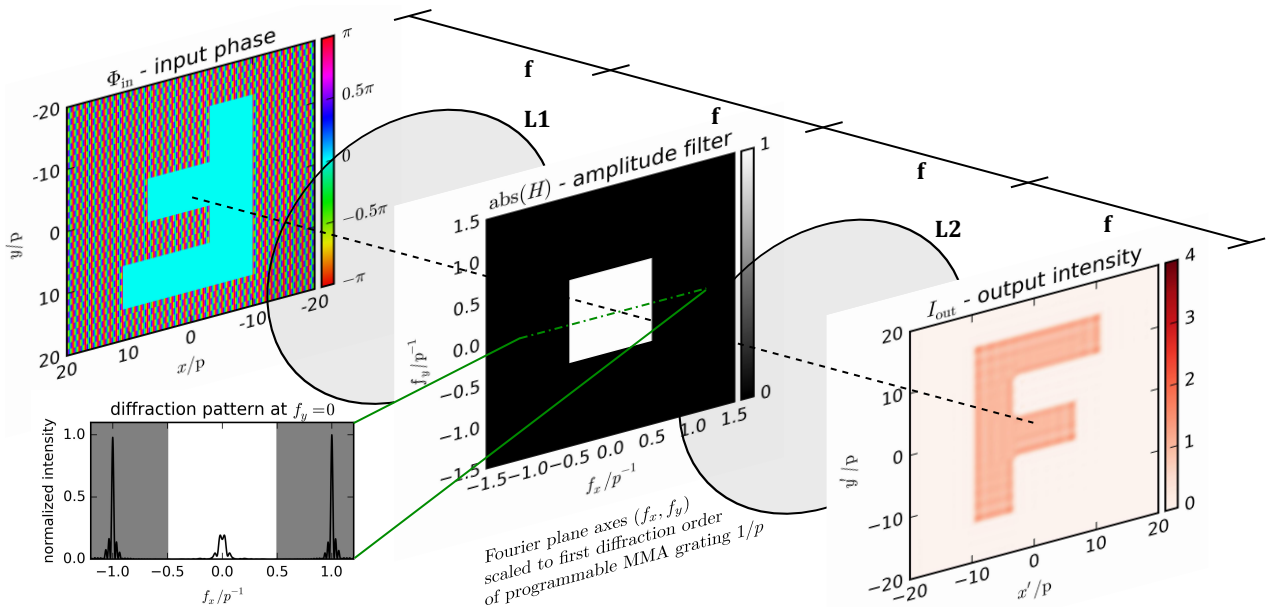

Figure 3: Numerical image formation with a tilt-type phase modulator in the image plane and a static amplitude filter in the Fourier plan. The input modulator has a size of $N_{\text{in}} * N_{\text{in}} = 40 * 40$ pixels of pitch p and is illuminated with a plane wave. The Fourier plane filter has a size of $\zeta = 0.5$ and absorbs the first and higher diffraction orders of the programmable MMA grating, as illustrated by the diffraction pattern.

3.2 Generalized Phase Contrast (GPC)

The Generalized Phase Contrast Method[9] is a conceptual generalization of Zernike's phase contrast Microscopy. It is suitable for the conversion of a phase pattern to an amplitude pattern. GPC's foundation lies in the separation of background and image wave in the Fourier plane. The desired pattern I_{des} will be inscribed to the phase modulator as its phase profile Φ_{in}. The phase profile is a scaled version of the desired intensity pattern I_{des}, which is normalized to the interval [0,4] relative to the intensity at the input[9]

$$|\Phi_{\text{in}}(x,y)| = 2\sin^{-1}\left(\frac{\sqrt{I_{\text{des}}(x',y')}}{2}\right) \ , \ u_{\text{in}}(x,y) = \exp\left(i\Phi_{\text{in}}(x,y)\right)\text{rect}\left(\frac{x}{L_x},\frac{y}{L_y}\right) \ . \tag{10}$$

Light without major phase structure will be distributed at low spatial frequencies in the Fourier plane. The phase shifting region of the GPC filter applies to this zero order light. The dimension of the filter $(f_{\eta,x}, f_{\eta,y})$ is in the order of the focal point's size accordingly (eq.(11)).[9] For most cases in GPC light shaping it is optimal to fix the phase shift of this filter to $\vartheta = \pi$ (eq.(12)).[9] We parameterize the size of the GPC filter for simulation with the scaling factor (η_x, η_y), according to the analytical expression in eq.(12)

$$H_{\text{GPC}}(f_x,f_y) = 1 + (\exp(i\vartheta) - 1)\,\text{rect}\left(\frac{f_x}{f_{\eta,x}},\frac{f_y}{f_{\eta,y}}\right) \tag{11}$$

$$\overset{\vartheta=\pi}{=} 1 - 2\,\text{rect}\left(\frac{f_x}{2\eta_x L_x^{-1}},\frac{f_y}{2\eta_y L_y^{-1}}\right) \text{ with } \eta_x = \frac{L_x f_{\eta,x}}{2},\ \eta_y = \frac{L_y f_{\eta,y}}{2} \ . \tag{12}$$

GPC light shaping relies on the constructive interference of the modulated pattern wave with the unmodulated background wave, the latter being turned into a so-called synthetic reference wave (SRW) $g(x',y')$. Both waves travel the same optical path. Therefore GPC belongs to the class of common-path-interferometers. If the filter is appropriately sized and precisely positioned on the optical axis the SRW will approach a nearly constant spatial distribution.[9] The SRW can then be described by a constant, its central value g_0. Analytically, g_0 can be

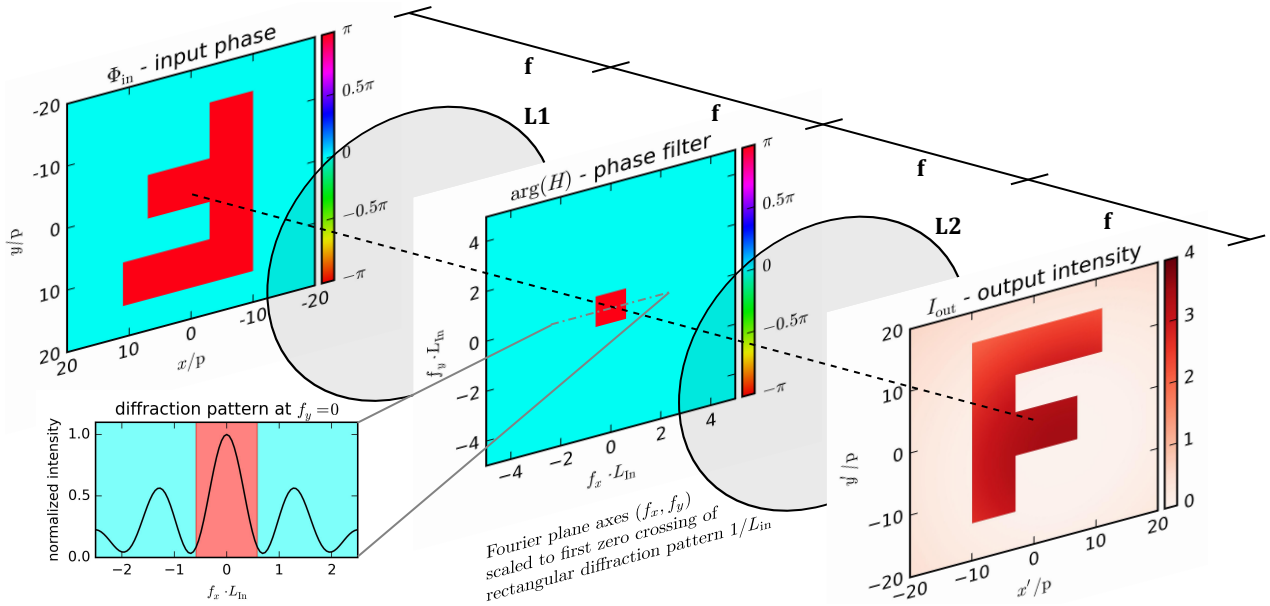

Figure 4: GPC simulation with two piston-type phase filters; pattern resolution of $N_{\text{in}} * N_{\text{in}} = 40 * 40$ pixels. The Fourier plane filter has the ideal size for this input pattern and shifts the phase at low spatial frequencies. The light is redistributed from the input plane (unity amplitude plane wave illumination) to the pattern shape in the output plane, where the intensity gain is up to 4. The desired pattern is uniform and has a fill factor of 25 %. This yields the complex spatial average $\bar{\alpha} = 0.5 + j0$ (see eq.(15)).

approximated as a direct function of the GPC filter size (η_x, η_y) using the sine integral function Si (see fig.5a):[20]

$$g(x', y') = \mathfrak{F}\left\{\text{rect}\left(\frac{f_x}{f_{\eta,x}}, \frac{f_y}{f_{\eta,y}}\right) \cdot \mathfrak{F}\left\{\text{rect}\left(\frac{x}{L_x}, \frac{y}{L_y}\right)\right\}\right\} \tag{13}$$

$$g_0(\eta_x, \eta_y) \approx \frac{4}{\pi^2}\text{Si}(\pi\eta_x)\text{Si}(\pi\eta_y)\ . \tag{14}$$

Optimum conditions in the context of GPC relate to a dark background and a uniform distribution of the SRW. For optimal GPC intensity shaping, two conditions based on the complex spatial average of the input wave have to be satisfied.[9] The complex spatial average, $\bar{\alpha}$, is calculated by means of the integrated input field:

$$\bar{\alpha} = \frac{1}{A}\iint_A u_{\text{in}}(x, y)\,\mathrm{d}x\,\mathrm{d}y = \bar{\alpha}_{\text{real}} + \mathrm{j}\bar{\alpha}_{\text{imag}} \tag{15}$$

$$\bar{\alpha}_{\text{imag}} \stackrel{!}{=} 0 \tag{16}$$

$$g_0(\eta) \cdot \bar{\alpha}_{\text{real}} \stackrel{!}{=} 0.5\ . \tag{17}$$

The condition on the imaginary part $\bar{\alpha}_{\text{imag}}$ in eq.(16) is always true for a uniform desired intensity, such as in our example in fig.4. Also in case that grayscale values shall be displayed, condition (16) can efficiently be fulfilled by suitable preprocessing of the input phase (refer to ref. 9).
The condition concerning the real part $\bar{\alpha}_{\text{real}}$ in eq.(17) is not trivial, because it is a function of the pattern fill factor via the complex spatial average. The normalized filter width η must be chosen according to the pattern fill factor to fulfill this condition. There always exists an optimal filter width based on the approximation of the SRW in eq.(14). The solution of the sine integral function in eq.(14) is not unique, but it is advantageous to restrict oneself to the filter diameters $\eta \in [0, 1]$,[9] for which the relationship is unambiguous (see fig. 5a). If the optimum condition in eqs.(16,17) is violated, the performance will be affected.

3.2.1 Fourier Plane filter size and position

Experimental studies of symmetrical patterns for GPC have demonstrated the significant influence of the size and position mismatch of the Fourier filter.[21] For the case of a non-symmetric pattern, figure 5b shows the change of the performance parameters as a function of the filter size for a set of simulations. It is apparent, that an optimum exists at $\eta \approx 0.6$, where $\bar{I}_{\text{pattern}}$ and ϵ reach a maximum. Figure 6 illustrates the intensity distribution at the output when violating the optimum condition eq.(17). Choosing η too small generates an offset intensity outside the desired pattern area. When choosing η too large the output intensity distribution becomes less uniform.

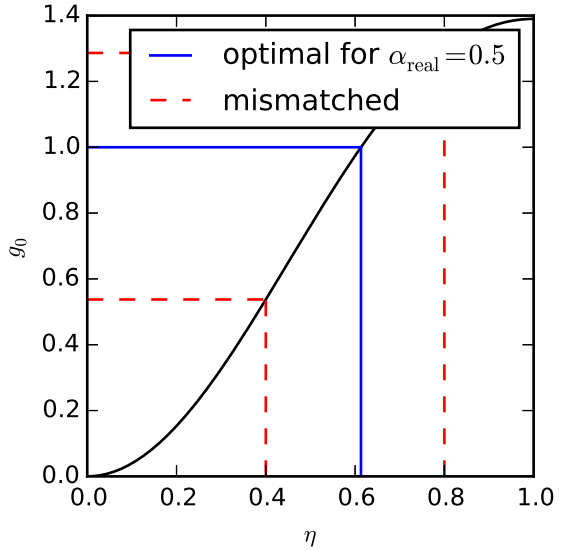

(a) SRW generating function g_0 for $\eta_x = \eta_y = \eta$ (see eq.(14)), with nominal value used in fig.4 (to satisfy eq.(17)) and mismatched values used for fig.6

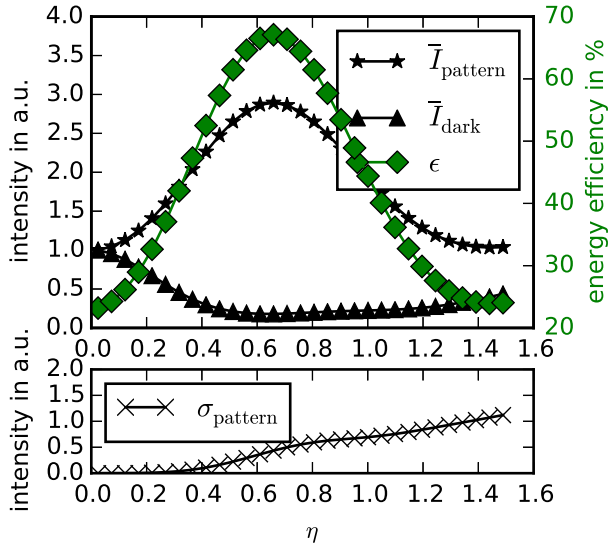

(b) Performance parameters as a function of the normalized GPC filter diameter η, for examplary pattern

Figure 5: Dependence of GPC on the normalized filter diameter

Since the GPC filter applies to zero order light, the method demands for strict centering of the phase filter on the optical axis. In figure 7 it can be seen how the error values increase with filter misalignment f_{shift}. The spatial frequency shift can also be expressed in the normalized filter dimensions introduced in eq.(12) ($\eta_{\text{shift}} = 0.5\, L_{\text{in}} \cdot f_{\text{shift}}$).

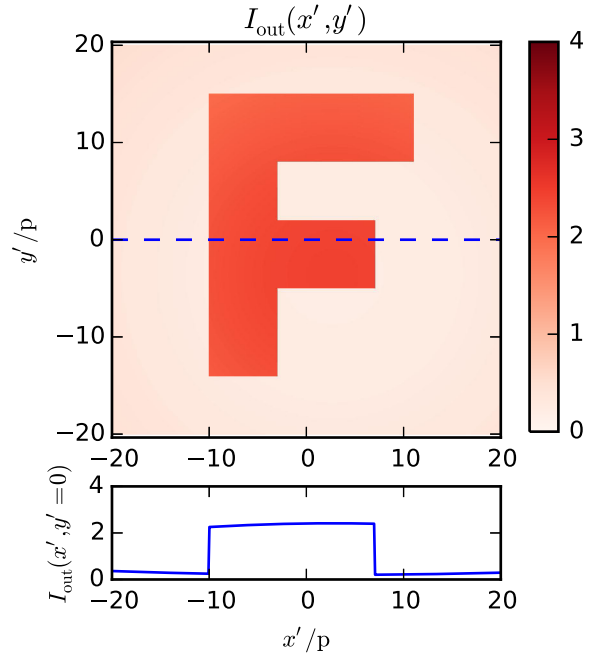

(a) Mismatched filter with $\eta = 0.4$

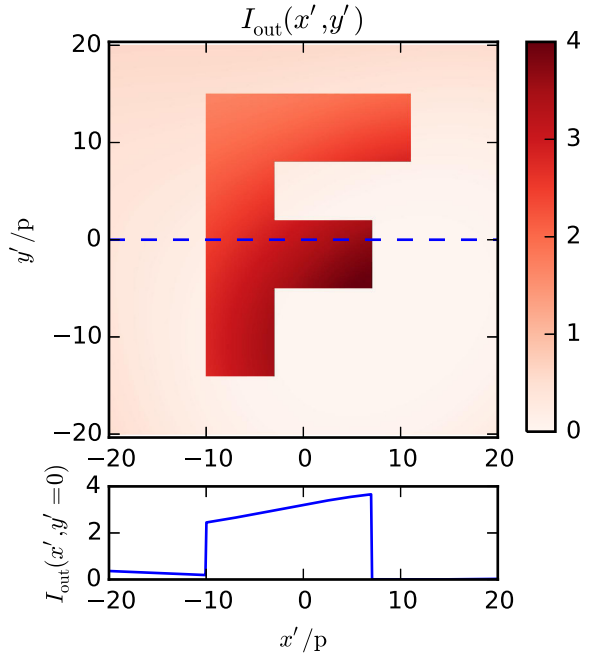

(b) Mismatched filter with $\eta = 0.8$

Figure 6: Intensity distributions for mismatched GPC filter sizes

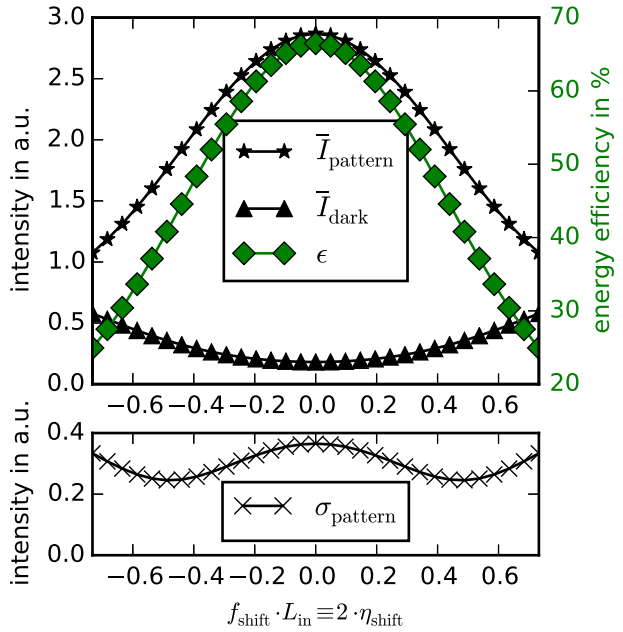

(a) Performance parameters as a function of filter displacement in the Fourier plane, at optimal filter diameter

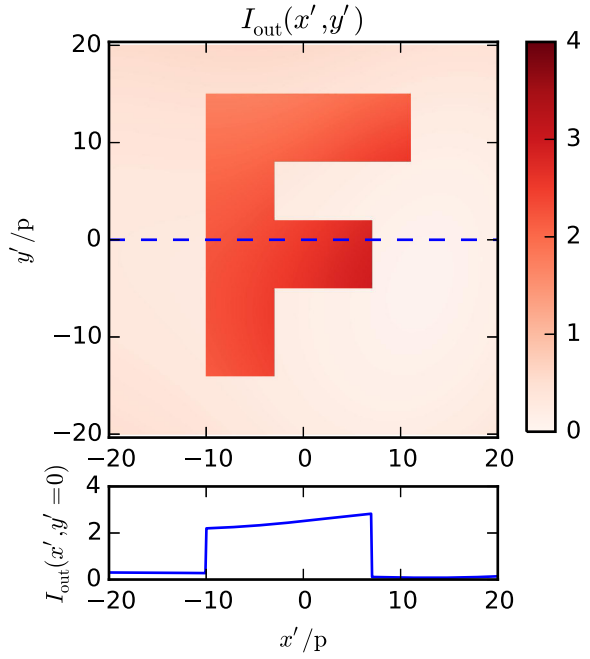

(b) Intensity distribution for $f_{\mathrm{shift}} = 0.342 \cdot 1/L_{\mathrm{in}}$

Figure 7: GPC influence of Fourier filter displacement

3.2.2 The variable GPC filter in the Fourier plane

We conclude from our simulation concerning the filter size mismatch (fig.5b) that general patterns of variable size require a programmable modulator for the realization of the corresponding GPC filter. In similar simulations we have seen that also the optical alignment is critical (fig.7a). A programmable modulator will be at least beneficial for the alignment because it enables fine re-positioning of the GPC filter via simple re-programming. Based on the spatial sensitivity investigated above it seems necessary that a phase shifting region of $\eta = 1$ should be sampled by at least 20*20 modulating elements to fulfill the optimum GPC conditions. Literature data with experimental studies on a double-pass configuration support this conclusion.[12] In terms of simulation, this means to fill the focal point with at least 20*20 discrete pixels. This requirement rules our numerical simulation (see sec.2). The required frequency domain sampling interval f_{samp} can be derived directly from the diffraction pattern of a rectangular aperture, whose zeroth diffraction order has the extent $[-L_{\mathrm{in}}^{-1}, L_{\mathrm{in}}^{-1}]$ in the spatial frequency domain,

$$f_{\mathrm{samp}} \simeq 0.1 \cdot \frac{1}{L_{\mathrm{in}}} \ . \tag{18}$$

Simultaneously, the effective image resolution is influenced by the size of the Fourier plane filter. For an input modulator of resolution $N_{\mathrm{in}} * N_{\mathrm{in}}$ the highest displayable frequency can be represented by a grating of spatial period $2p$, with its fundamental spatial frequency $f_{\mathrm{in,max}}$ (eq.(19)). A programmable modulator in the Fourier plane of resolution $N_{\mathrm{F}} * N_{\mathrm{F}}$ and discrete sampling interval f_{samp} will have a frequency bandwidth of $f_{\mathrm{B}} = N_{\mathrm{F}} \cdot f_{\mathrm{samp}}$. If the full resolution capability of the input modulator is to be preserved at the output, the frequency bandwidth of the Fourier plane filter will need to cover $f_{\mathrm{in,max}}$:

$$f_{\mathrm{in,max}} = \frac{1}{2p} = \frac{N_{\mathrm{in}}}{2L_{\mathrm{in}}} \tag{19}$$

$$f_{\mathrm{B}} \overset{!}{\geq} 2 f_{\mathrm{in,max}} = 1\, p^{-1} \ . \tag{20}$$

Including the requirement on the spatial sampling of the focal point from eq.(18), we see that the Fourier plane field should be more precisely sampled than the image plane by a factor of about 10 in both spatial directions (f_x, f_y). In other words the pixel number of the Fourier plane filter should be $(10 \cdot 10 = 100)$ times higher than the input modulator.

$$N_{\mathrm{F}} \cdot f_{\mathrm{samp}} \overset{!}{\geq} 2\frac{N_{\mathrm{in}}}{2L_{\mathrm{in}}} \ \rightarrow \ \frac{N_{\mathrm{F}}}{N_{\mathrm{in}}} \overset{!}{\geq} 10 \tag{21}$$

As discussed in sec.2 the image quality directly depends on the total size of the programmable Fourier plane filter. Combining sufficient zero order sampling and the condition to preserve the imaging quality places a significant system design aspect on the choice of the Fourier plane modulator. If two modulators of identical resolutions are to be used, the system designer will have the option to restrict the displayable pattern to low spatial frequencies, as has been done in a previous study.[12] However, this restriction does not comply with our criteria for a universal GPC imaging application.

4. GENERATION OF MULTIPLE SPOTS

In this section we apply the matched filter technique[13] within the Generalized Phase Contrast context (mGPC) for the generation of multiple spots. The intensity peaks are created here by an optical operation similar to autocorrelation.[14] Matched filtering is way to detect a phase object in the input plane by applying an adapted filter in the Fourier plane. The phase object can have an arbitrary distribution. For illustration, we simulate a tilt mirror array with mGPC in section 4.2. Correlation peaks represent local maxima of the output intensity. Relevant figures of merit are the mean of the peak intensities $\overline{I}_{\mathrm{peak}}$ and their variation,σ_{peak}, in this section

$$\overline{I}_{\mathrm{peak}} = \mathrm{mean}\left(I_{\mathrm{out}}(x', y')|_{(x',y') \in \text{ local maxima}} \right) \tag{22}$$

$$\sigma_{\mathrm{peak}} = \mathrm{std}\left(I_{\mathrm{out}}(x', y')|_{(x',y') \in \text{ local maxima}} \right) \ . \tag{23}$$

The numerical values of the peak intensities in correlation filtering strongly depend on the spatial sampling of the output plane. We continue to use the parameters of sec.2 consistently. In practice the achievable peak intensities will be limited by the various system apertures. We illustrate this effect by means of the Fourier plane bandwidth f_{B}, in a set of simulations.

4.1 Matched Filter Generalized Phase Contrast (mGPC)

The input phase for mGPC consists of a set of N identical user-specified phase correlation targets $\Phi_{\mathrm{T}}(x, y)$ (eq.(24)). Their centers $(x_{\mathrm{p},k}, y_{\mathrm{p},k})$ mark the locations of the correlation peaks at the output. A matched filter is determined by the Fourier transform of the phase target. For mGPC the matched filter for a phase target is combined with a GPC filter (eq.(25)). These two phase filters can be implemented advantageously on the same modulator,[14] because they each apply either exclusively to low spatial frequencies (GPC) or mostly to high spatial frequencies (correlation). As a result, the GPC term distributes light to the pattern area and the correlation term creates point spots at the output. Figure 8 shows that the mGPC point spots may reach higher values than the input wave by two orders of magnitude

$$\Phi_{\mathrm{in}}(x, y) = \sum_{k=1}^{N} \Phi_{\mathrm{T}}(x - x_{\mathrm{p},k}, y - y_{\mathrm{p},k}) \tag{24}$$

$$H_{\mathrm{mGPC}}(f_x, f_y) = \arg\left(\mathfrak{F}(u_{\mathrm{T}}(x, y))\right) \cdot H_{\mathrm{GPC}}(f_x, f_y) \cdot \mathrm{rect}\left(\frac{f_x}{f_{\mathrm{B}}}, \frac{f_y}{f_{\mathrm{B}}}\right) \text{ with } u_{\mathrm{T}} = \exp(j\Phi_{\mathrm{T}}) \ . \tag{25}$$

mGPC's performance parameters strongly depend on both the choice of target pattern Φ_{T} and the spatial extent of the Fourier plane phase filter. To illustrate the latter property, figure 9 shows the result of a set of simulations, where the Fourier filter bandwidth f_{B} was varied. The peak intensities show a nearly linear dependence on f_{B}.

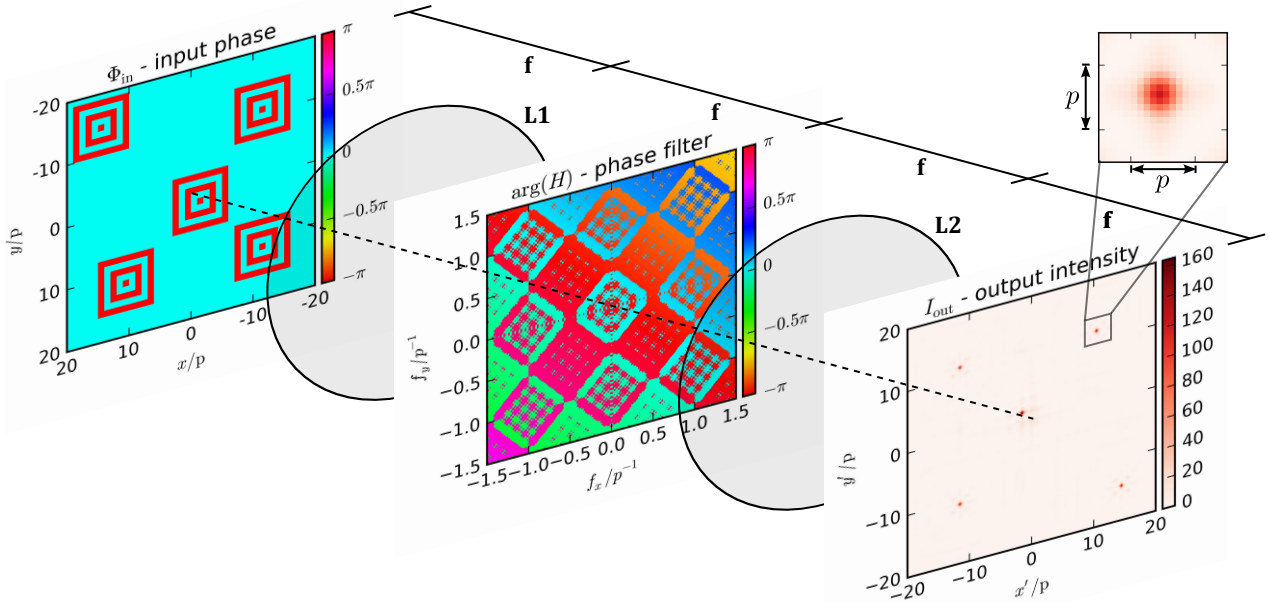

Figure 8: Numerical simulation of mGPC, with piston-type phase filters in the image and in the Fourier plane. The input pattern has a resolution of $N_{\mathrm{in}} * N_{\mathrm{in}} = 40 * 40$ pixels of pitch p and the Fourier plane filter has a bandwidth $f_{\mathrm{B}} = 3\,p^{-1}$. The GPC filter has the optimal size for our input pattern with $\overline{\alpha} = 0.694 + j0$. Light is concentrated in correlation peaks, whose position is determined by the phase targets.

For an optimal mGPC design, the filter function H_{mGPC} (see eq.(25)) needs to be adapted if either the correlation target Φ_{T} or complex average of the input wave, $\overline{\alpha}$, change. The complex average $\overline{\alpha}$ is a function of

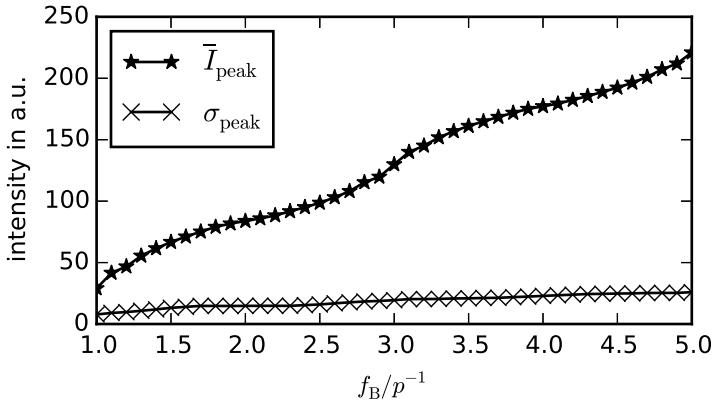

Figure 9: Mean peak intensities and their standard deviation as a function of the Fourier plane filter bandwidth f_{B} for mGPC multispot generation. These simulations were carried out using the same set of parameters as in fig.8, including the phase target.

the pattern fill factor and thereby related to the amount of correlation targets k. If one chooses to implement the Fourier filter with a phase-only SLM the sampling constraints of GPC in eq.(21) will apply in addition to the bandwidth requirement explained above. According to fig.9, a larger bandwidth of $3\,p^{-1}$ becomes suitable for higher spot intensity. This clearly indicates a strong increase of the necessary Fourier filter area, compared to GPC ($\sim 1\,p^{-1}$). As a consequence, the corresponding requirement for the number of modulator elements increases by almost an order of magnitude.

4.2 Matched Filter GPC with tilt mirror arrays

Fig. 10 illustrates the mGPC simulation of high-intensity spots with a tilt-type phase modulator. Compared to the piston type modulation in figure 8 we obtain sharper correlation peaks and comparable peak intensities with tilt mirror modulation. The increased sharpness of the correlation peaks can be attributed to the high spatial frequencies in the input pattern introduced by the tilt mirrors.
The GPC portion of the Fourier filter has been selected optimally for both modulation types, but not identical. We have used identical addressing schemes, but the complex spatial average of a single pixel is in principle smaller for tilt mirrors ($\overline{\alpha}_{\mathrm{pixel}} = 0$ instead of $\overline{\alpha}_{\mathrm{pixel}} = -1$ for a piston type pixel in the pattern). Therefore the global complex average $\overline{\alpha}$ is higher in case of tilt mirror modulation. This is a numerical description of the fact, that the portion of the image considered as the 'background wave' is stronger in tilt modulation, while the 'image part' is weaker. Nonetheless, supposed the GPC part of the mGPC filter is adjusted appropriately, the setups may perfectly create the desired correlation spots for both types of modulators at high speed.

5. SYSTEM COMPARISON AND DISCUSSION

In this paper we have investigated system design aspects for the use 4f phase modulation techniques for spatial beam shaping. All techniques possess an analytical input-output-relationship and therefore support high modulation update rates. After illustration of the versatile, industrial technique for maskless lithography using tilt micro mirror arrays (MMAs) we have considered the Generalized Phase Contrast (GPC) because of its high energy efficiency and its intensity gain with respect to the input illumination. Both pattern modulation techniques enable the projection of speckle-free, continuous patterns.

Table 1 shows our system level comparison of the two methods relevant for pattern generation. The MMA modulation with fixed, absorbing Fourier filter succeeds in achieving near-zero intensity where this is desired (i.e. high image contrast). The low mean intensity outside the pattern illustrates this. MMA modulation places no pattern specific constraints on the Fourier filter. Since it is an amplitude filtering technique its energy efficiency is limited.

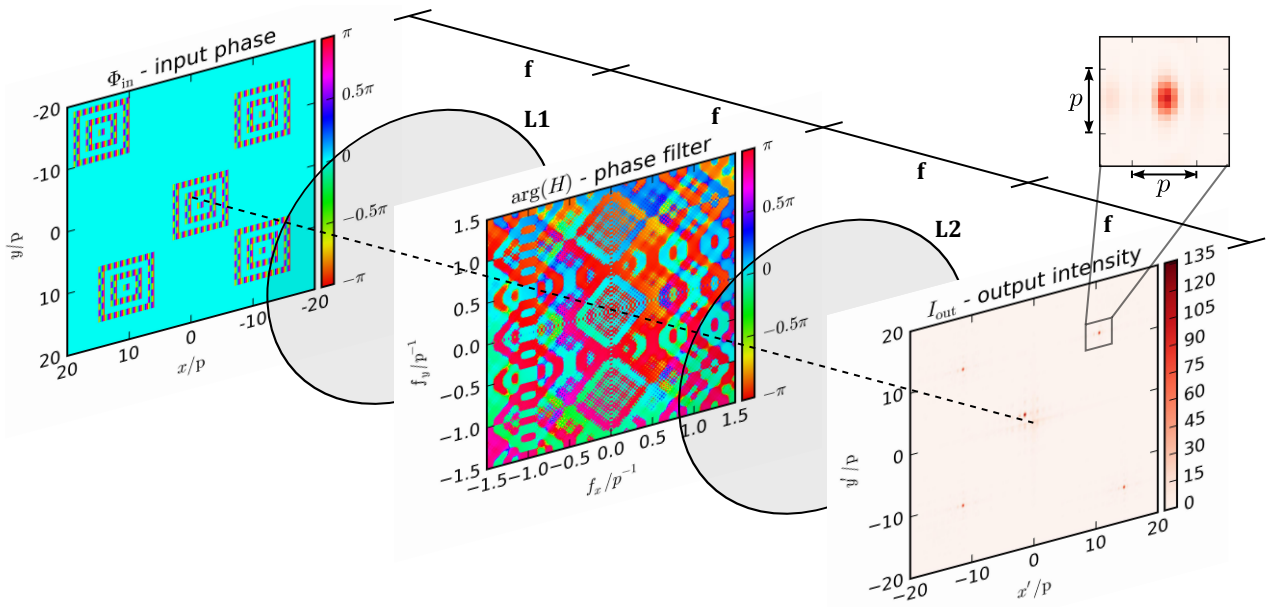

Figure 10: Numerical simulation of mGPC, with a tilt-type phase modulator in the image plane and a piston-type modulator in the Fourier plane. The input pattern has a resolution of $N_{\text{in}} * N_{\text{in}} = 40 * 40$ pixels of pitch p and the Fourier plane filter has a bandwidth $f_{\text{B}} = 3\,p^{-1}$. The GPC filter has the optimal size for our input pattern with $\overline{\alpha} = 0.847 + j0$.

GPC on the other hand clearly may distribute more intensity into the pattern area and therefore triples the energy efficiency. For the non-symmetric pattern in our analysis, a notable share of the light goes, however, to positions outside the desired pattern and reduces the image contrast by more than a factor of 4. Also to note, the intensity variation within pattern is slightly higher than that of MMA modulation with amplitude filter. All results in table 1 refer to ideal operating conditions. As a consequence of our boundary to consider patterns with arbitrary size, GPC requires a second phase-only SLM to reach these performance values.

Table 1: System level comparison of 4f pattern generation methods considered in this paper

	MMA	**GPC**
mean pattern intensity $\overline{I}_{\text{pattern}}$	0.939	2.87
mean intensity outside pattern $\overline{I}_{\text{dark}}$	0.0139	0.181
contrast ratio $(\overline{I}_{\text{pattern}}/\overline{I}_{\text{dark}})$	67.6	15.9
variation of the pattern σ_{pattern}	0.209	0.365
energy efficiency ϵ	21.8 %	66.5 %
pattern specific Fourier plane filter constraints	none	Filter size (sec. 3.2.1)
effective resolution (Fourier plane bandwidth)	$f_{\text{B}} = 2\zeta \cdot p^{-1}$ (refer to eq.(9))	for programmable filter*: $f_{\text{B}} \approx 0.1\frac{N_{\text{F}}}{N_{\text{in}}} \cdot p^{-1}$ (refer to eq.(21))
data set for performance parameters	fig.3	fig.4

The pixel number of this second modulator will have to be much higher than the input modulator's, by about two orders of magnitude, as we have discussed in section 3.2.2. Apart from the particular system complexity, the second SLM has to modulate the zero order in the focal point of the first lens. The focal point intensity will

*second programmable phase-only SLM with resolution $N_{\text{F}} * N_{\text{F}}$ in the Fourier plane

become significant in high power applications with respect to the modulator's damage threshold.[22] Consequently, the GPC approach inherently bears a challenge for the beam shaping of higher laser intensities.

After investigating 4f pattern projection we have considered the matched filter GPC (mGPC). Table 2 compares the figures of merit for the spot generating technique, which we have introduced in eqs.(22,23). We have simulated mGPC with piston and, for the first time, tilt-type MMAs in the image plane.
With respect to the spot peak intensity, mGPC clearly is a very attractive beam shaping method. Nevertheless, the design requirements derived for GPC retain their validity. For a system, which is flexible with respect to the amount of spots and the phase target, the Fourier plane modulator should be programmable. This second phase-only SLM needs a higher resolution than the initial object modulator by more than a factor of 100 in order to support a sufficient imaging bandwidth. The speed advantage of the very attractive mGPC (partially GPC) compared to holographic 2f methods for beam shaping therefore seems to be associated with a certain system-challenge on the optical modulator side.

Table 2: System level comparison of mGPC modulation for the generation of multiple spots with different input modulators

	mGPC with piston/piston modulators	**mGPC with tilt/piston modulators**
mean peak intensity $\overline{I}_{\text{peak}}$	130	105
peak variation σ_{peak}	19.4	17.9
data set for performance parameters	fig.8	fig.10

ACKNOWLEDGMENTS

We gratefully acknowledge financial support from the TU Dresden Graduate Academy in the form of a travel grant to the conference.

REFERENCES

[1] Auyeung, R. C. Y., Kim, H., Charipar, N. A., Birnbaum, A. J., Mathews, S. A., and Piqué, A., "Laser forward transfer based on a spatial light modulator," *Applied Physics A* **102**, 21–26 (Jan. 2011).

[2] Vaezi, M., Seitz, H., and Yang, S., "A review on 3d micro-additive manufacturing technologies," *The International Journal of Advanced Manufacturing Technology* **67**, 1721–1754 (July 2013).

[3] Poon, T.-C. and Liu, J.-P., [*Introduction to modern digital holography : with MATLAB*], Cambridge University Press, Cambridge, repr. with corrections ed. (2014).

[4] Zwick, S., Haist, T., Warber, M., and Osten, W., "Dynamic holography using pixelated light modulators," *Appl. Opt.* **49**, F47–F58 (Sept. 2010).

[5] Shimobaba, T., Weng, J., Sakurai, T., Okada, N., Nishitsuji, T., Takada, N., Shiraki, A., Masuda, N., and Ito, T., "Computational wave optics library for C++: CWO++ library," *Computer Physics Communications* **183**(5), 1124–1138 (2012).

[6] Shimobaba, T. and Ito, T., "Random phase-free computer-generated hologram," *Optics Express* **23**, 9549 (Apr. 2015).

[7] Sandstrom, T., Askebjer, P., Sallander, J., Zerne, R., and Karawajczyk, A., "Pattern generation with SLM imaging," in [*Proceedings of SPIE*], **4562**, 38–44 (2002).

[8] Heber, J., Kunze, D., Dürr, P., Rudloff, D., Wagner, M., Björnängen, P., Luberek, J., Berzinsh, U., Sandström, T., and Karlin, T., "Contrast properties of spatial light modulators for microlithography," in [*Proceedings of SPIE*], Naber, R. J. and Kawahira, H., eds., **6730**, 673035–673035–10 (Oct. 2007).

[9] Glückstad, J. and Palima, D., [*Generalized phase contrast / applications in optics and photonics*], no. 146 in Springer series in optical sciences, Springer (2009).

[10] Bañas, A., Palima, D., Villangca, M., Aabo, T., and Glückstad, J., "GPC light shaper for speckle-free one- and two-photon contiguous pattern excitation," *Optics Express* **22**, 5299 (Mar. 2014).

[11] Palima, D. and Glückstad, J., "Comparison of generalized phase contrast and computer generated holography for laser image projection," *Optics express* **16**(8), 5338–5349 (2008).

[12] Kenny, F., Choi, F., Glückstad, J., and Booth, M., "Adaptive optimisation of a generalised phase contrast beam shaping system," *Optics Communications* **342**, 109–114 (May 2015).

[13] Horner, J. L. and Gianino, P. D., "Phase-only matched filtering," *Applied optics* **23**(6), 812–816 (1984).

[14] Bañas, A., Palima, D., and Glückstad, J., "Matched-filtering generalized phase contrast using LCoS picoprojectors for beam-forming," *Optics express* **20**(9), 9705–9712 (2012).

[15] Gehner, A., Wildenhain, M., Neumann, H., Knobbe, J., and Komenda, O., "MEMS analog light processing: an enabling technology for adaptive optical phase control," in [*Proceedings of SPIE*], Olivier, S. S., Tadigadapa, S. A., and Henning, A. K., eds., **6113**, 61130K–61130K–15 (Jan. 2006).

[16] Schmidt, J.-U., Bring, M., Heber, J., Friedrichs, M., Rudloff, D., Rößler, J., Berndt, D., Neumann, H., Kluge, W., Eckert, M., List, M., Müller, M., and Wagner, M., "Technology development of diffractive micromirror arrays for the deep ultraviolet to the near infrared spectral range," in [*Proceedings of SPIE*], Thienpont, H., Van Daele, P., Mohr, J., and Zappe, H., eds., **7716**, 77162L–77162L–10 (Apr. 2010).

[17] Goodman, J. W., [*Introduction to Fourier optics*], Roberts, Englewood, Colo., 3. ed. ed. (2005).

[18] Liu, J.-P., "Controlling the aliasing by zero-padding in the digital calculation of the scalar diffraction," *JOSA A* **29**(9), 1956–1964 (2012).

[19] Voelz, D., [*Computational Fourier Optics - A Matlab Tutorial*], vol. TT89 of *Tutorial Texts in Optical Engineering*, SPIE Press, Bellingham, Washington (USA) (2011).

[20] Alonzo, C. A., Rodrigo, P. J., and Glückstad, J., "Photon-efficient grey-level image projection by the generalized phase contrast method," *New Journal of Physics* **9**, 132–132 (May 2007).

[21] Bañas, A., Kopylov, O., Villangca, M., Palima, D., and Glückstad, J., "GPC light shaper: static and dynamic experimental demonstrations," *Optics Express* **22**, 23759 (Oct. 2014).

[22] Beck, R. J., Parry, J. P., MacPherson, W. N., Waddie, A., Weston, N. J., Shephard, J. D., and Hand, D. P., "Application of cooled spatial light modulator for high power nanosecond laser micromachining," *Optics express* **18**(16), 17059–17065 (2010).